Dislocation dynamics in Al-Mg-Zn alloys

Hosson, J.Th.M. De; Kanert, O.; Schlagowski, U.; Boom, G.

Published in:
Journal of Materials Research

DOI:
10.1557/JMR.1988.0645

Publication date:
1988

Dislocation dynamics in Al–Mg–Zn alloys: A nuclear magnetic resonance and transmission electron microscopic study

J. Th. M. De Hosson
Department of Applied Physics, Materials Science Centre, University of Groningen, Nijenborgh 18, 9747 AG Groningen, The Netherlands

O. Kanert and U. Schlagowski
Institute of Physics, University of Dortmund, 46 Dortmund 50, Federal Republic of Germany

G. Boom
Department of Applied Physics, Materials Science Centre, University of Groningen, Nijenborgh 18, 9747 AG Groningen, The Netherlands

(Received 16 December 1987; accepted 29 February 1988)

Pulsed nuclear magnetic resonance (NMR) proved to be a complementary new technique for the study of moving dislocations in Al–Mg–Zn alloys. The NMR technique, in combination with transmission electron microscopy (TEM), has been applied to study dislocation motion in Al–0.6 at. % Mg–1 at. % Zn and Al–1.2 at. % Mg–2.5 at. % Zn. Spin-lattice relaxation measurements clearly indicate that fluctuations in the nuclear quadrupolar interactions caused by moving dislocations in Al–Mg–Zn are different compared to those in ultra pure Al. From the motion induced part of the spin-lattice relaxation rate the mean jump distance of mobile dislocations has been determined as a function of strain. From the NMR data it is concluded that moving dislocations advance over a number of solute atoms in these alloys as described by Mott–Nabarro's model. At large strains there exists a striking difference between the mean jump distances in Al–0.6 at. % Mg–1 at. % Zn and in Al–1.2 at. % Mg–2.5 at. % Zn. The latter is about five times smaller than the former one. This is consistent with TEM observations that show dislocation cell formation only in Al–0.6 at. % Mg–1 at. % Zn and the macroscopic stress–strain dependences of these alloys.

I. INTRODUCTION

In this investigation we will focus mainly on plastic deformation experiments at a constant strain rate $\dot{\epsilon}$. This type of situation is governed by Orowan's equation,[1] where the strain rate is linearly proportional to L/τ_m. Here L is the mean jump distance of dislocations and τ_m represents the mean time of stay of a dislocation in front of an obstacle. A few years ago, we showed that pulsed nuclear magnetic resonance (NMR) is a useful tool for studying dislocation motion under constant strain rate conditions. It turned out that the mean jump distance of dislocations could be deduced from these measurements. For detailed information of this technique, reference is made to our review paper.[2] Only a concise summary will be presented here.

The method is essentially based on the interaction between nuclear electric quadrupole moments and elastic-field gradients at the nucleus. Around a dislocation in a cubic crystal the symmetry is destroyed and interactions between nuclear electric quadrupole moments and electric-field gradients arise. Whenever a dislocation changes its position in the crystal, the surrounding atoms have also to move, thus causing time fluctuations of the quadrupolar spin Hamiltonian for spins with $I > \frac{1}{2}$. Furthermore, for the investigation of rather infrequent defect motions as in the case of moving dislocations, the spin-lattice relaxation time in a weak rotating frame, $T_{1\rho}$, has proved to be the most appropriate NMR parameter affected by such motions because the "time windows" of $T_{1\rho}$ lie in the range of τ_m.

Using sufficiently small deformation rates $\dot{\epsilon}$, so that $1/\tau_m \ll \omega$, the Larmor frequency in the rotating frame, the dislocation-induced relaxation rate is given by[2]

$$\frac{1}{T_{1\rho}} = \frac{A_Q}{H_1^2 + H_{L\rho}^2} \frac{1}{bL} \dot{\epsilon}\,, \tag{1}$$

where A_Q depends on the mean-squared electric-field gradient due to the stress field of a dislocation of unit length and the quadrupolar coupling constant. Here $H_{L\rho}$ is the mean local field in the rotating frame and H_1 is the (weak rotating) applied field; b represents the magnitude of the Burgers vector. Since A_Q and $H_{L\rho}$ can be determined separately,[2,3] for a given plastic deformation rate $\dot{\epsilon}$ the spin-lattice relaxation rate can be used to determine L as a function of a physical parameter as strain. It has to be emphasized that the observed spin-lattice relaxation rate is a sum of $1/T_{1\rho}$ [Eq. (1)] and a background relaxation rate $1/T_{1\rho}^0$. The background relaxation that is caused in metallic samples by conduction electrons (Korringa relaxation) can easily be determined by setting $\dot{\epsilon} = 0$ in the actual NMR experiment.

 0003-6951/88/040645-06$01.75

II. EXPERIMENTAL

Polycrystalline samples with a grain size of the order of 100 μm were used. To avoid skin effect distortion of the NMR signal, the actual NMR experiment was carried out on a single rectangular foil of size 27 mm × 12 mm × 40 μm. Three sets of polycrystalline samples were used: ultrapure (5*N*) Al, Al–0.6 at. % Mg–1 at. % Zn, and Al–1.2 at. % Mg–2.5 at. % Zn. The starting material for the different samples was homogenized at 550 °C for 3 days, the material was rolled out to thin foils, and it was cut by spark erosion to the sample size mentioned before. The 5*N* Al samples were annealed a second time at 290 °C for 1 h, whereas the alloys were exposed to the following procedure: annealing at 450 °C and quenched in water.

The NMR experiments discussed here are carried out at $T = 77$ K. At such a low temperature, nuclear spin relaxation effects because of diffusive atomic motions are negligible. In this case the correlation times for diffusive atomic jumps are much longer than the typical values of the waiting time τ_m of mobile dislocations that are about 10^{-4} s for $\dot{\epsilon} \simeq 1.5\ s^{-1}$. Consequently, an observable contribution of diffusive atomic motions to the measured spin-lattice relaxation rate does not occur.

In the NMR experiments, the sample under investigation is plastically deformed at a constant strain rate of about 1.5 s^{-1} by a servohydraulic tensile machine.[4] While the specimen is deforming ^{27}Al, the nuclear spin-relaxation rate $T_{1\rho}^{-1}$ is measured at an operating frequency of 15.7 MHz using the spin-locking technique.[5] Simultaneously, the actual deformation ϵ is observed. Before and after each experimental run, the background relaxation rate is measured by setting $\dot{\epsilon} = 0$.

Transmission electron micrographs are taken by using a JEM 200 CX. Disk-type specimens are taken from the deformed foils by spark cutting to minimize deformation. The samples are electrochemically thinned in a polishing equipment at room temperature in a solution of 49% methanol, 49% nitric acid, and 2% hydrochloric acid.

III. RESULTS AND DISCUSSION

The strain dependence of L has been obtained by measuring ($T_{1\rho}^{-1}$) as a function of strain ϵ. The results of ultrapure Al and the various ternary Al–Mg–Zn alloys are depicted in Fig. 1. The mean jump distance measured by NMR in pure Al has been published elsewhere.[3] In order to reduce statistical errors, each measurement was repeated about ten times and the average value of L is plotted in Fig. 1. These results demonstrate a decrease of L with increasing ϵ as expected from a general consideration in terms of deformation-created obstacles. For large values of ϵ, the mean jump distance approaches a minimum value $L_{\min}$ listed in Table I.

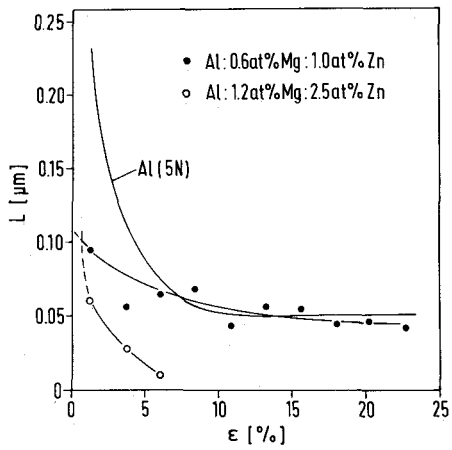

FIG. 1. The mean jump distance of mobile dislocations measured by NMR as a function of strain ϵ in (a) pure Al, (b) Al–0.6 at. % Mg–1 at. % Zn (●), and (c) Al–1.2 at. % Mg–2.5 at. % Zn (○).

There appears to be quite a difference among the various ternary alloys indicating that the dislocation microstructure might be considerably different. This was examined by taking TEM images of the dislocation configuration of the deformed samples as shown in Figs. 2(a)–2(c). The Al–0.6 at. % Mg–1.0 at. % Zn [Fig. 2(b)] shows a pronounced dislocation cell structure similar to that observed in deformed Al [Fig. 2(a)]. The corresponding histogram of the interspacing distances between the imaged dislocations is presented in Fig. 3(a), leading to a most probable value of about 0.04 μm (see Table I). In order to compare L_H with the mean jump distance L obtained by the *in situ* NMR experiments (Table I), one has to bear in mind that moving dislocations are hindered in their glide plane by different types of obstacles: forest dislocations present in the cell wall, dislocations in the interior region of the cell, and solute atoms. Assuming different sets of corresponding mobile dislocation densities ρ_i, the total spin-lattice relaxation rate can be decomposed in the separate contributions and, according to Eq. (1),

$$\frac{1}{T_{1\rho}} \approx \sum_i \frac{\rho_i}{L_i \rho} . \qquad (2)$$

TABLE I. Mean jump distances L at large strain values as obtained from the NMR measurements (Fig. 1, $L_{\min}$) and from the TEM observations as presented in Fig. 3 (L_H).

Sample	Al (5*N*)	Al–2.6 at. % Mg–1 at. % Zn	Al–1.2 at. % Mg–2.5 at. % Zn
$L_{\min}$ (μm)	0.05	0.043	$\lesssim$0.01
L_H (μm)	···	0.037	0.016

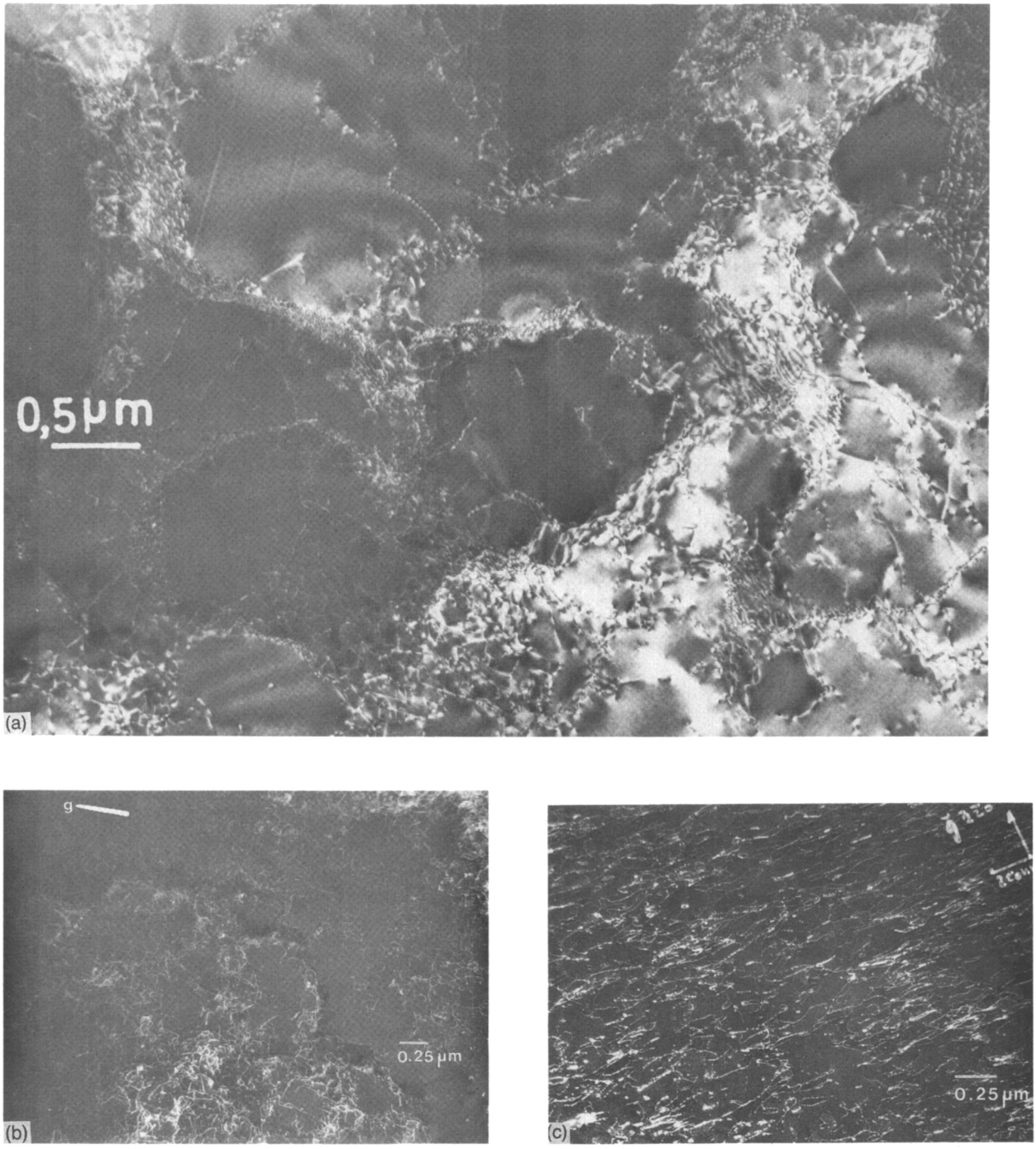

FIG. 2. Transmission electron micrograph of material deformed at 77 K: (a) aluminum ($g = 200$) until fracture, (b) Al–0.6 at. % Mg–1 at. % Zn ($g = 2\bar{2}0$) until $\epsilon = 20\%$, (c) Al–1.2 at. % Mg–2.5 at. % Zn ($g = \bar{2}20$) until fracture.

Taking ρ_i/ρ to be a constant value it is quite clear from Eq. (2) that the experimentally measured spin-lattice relaxation rate is mainly determined by the smallest L value. Consequently, in the case of a cell structure it means that the spin-lattice relaxation is connected to the spacing between forest dislocations inside the cell wall, which is smaller than the cell size and the distance between the solute atoms. So, the conclusion can be drawn that the $L_{\min}$ value of 0.043 μm by NMR (Table I) is governed by the mean interspacings of forest dislocations inside the cell wall (0.037 μm).

To the contrary, as demonstrated by the TEM observation (Fig. 2), the deformed Al–1.2 at. % Mg–2.5 at. % Zn does not exhibit a distinct cell structure, but

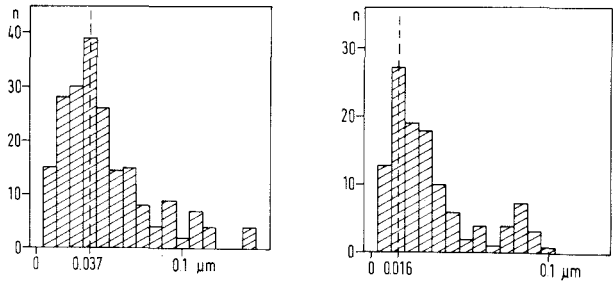

FIG. 3. Histograms of the distribution of interspacing dislocation distances as obtained from TEM images shown in Fig. 2: (a) Al–0.6 at. % Mg–1 at. % Zn and (b) Al–1.2 at. % Mg–2.5 at. % Zn.

rather a uniform distribution of dislocations. Obviously, the higher Mg and Zn content impedes the formation of a dislocation cell structure during the deformation process; this alloying effect is well known for a large number of fcc metals. The value of L_H (0.016 μm) [Fig. 3(b)] agrees fairly well with the mean jump distance of L_{min} obtained from NMR experiments (Table I). Consequently, we may conclude that the forest dislocations produced during deformation act as strong obstacles for the movement of mobile dislocations, in front of which spin-lattice relaxation takes place.

In order to explain the mean jump distance at small ϵ and its strain dependence, we separate the contribution to the spin-lattice relaxation rate due to weak obstacles like solute atoms and due to strong obstacles like forest dislocations. One can envision that at the yield stress level in the case of dilute alloys a small fraction of the primary dislocations must move through the weak obstacle field presented by the solutes before encountering forest dislocations. The mean jump distance can be written [see Eq. (2)] as

$$\frac{1}{L_{\mathrm{NMR}}} = \frac{\rho_1}{\lambda_F \rho} + \frac{\rho_2}{l_s \rho}, \tag{3}$$

where λ_F and l_s are the effective obstacle spacing between forest dislocations and solute atoms, respectively. In order to verify this expression we make the necessary assumption that the dislocation microstructure is the same in ultrapure Al and in the dilute Al–Mg–Zn alloys at a certain value of ϵ. This implies that $L_{\mathrm{NMR}}{}^{-1}$ (alloys) vs $L_{\mathrm{NMR}}{}^{-1}$ (pure Al) is a straight line. In Fig. 4 $L_{\mathrm{NMR}}{}^{-1}$ vs $L_{\mathrm{NMR}}{}^{-1}$ (pure Al) is depicted for both alloys and the pure material. At the beginning of deformation of the alloys $\rho_2/\rho \simeq 1$ (assuming that the two different fractions of mobile dislocation densities are proportional to the corresponding ratios of the effective planar obstacle densities).

This means that, at the smallest degree of deformation ($\epsilon = 1.25\%$) measured by NMR, l_s is found to be decreasing from 0.10 μm in Al–0.6 at. % Mg–1 at. % Zn to 0.07 μm in Al–1.2 at. % Mg–2.5 at. % Zn.

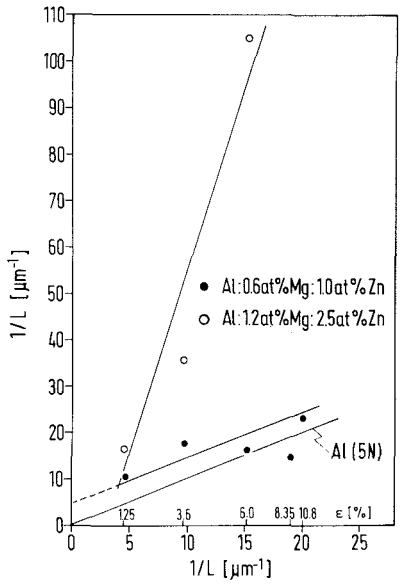

FIG. 4. Inverse of mean jump distance in Al–Mg–Zn alloys versus the same quantity in ultrapure (5*N*) Al as obtained from the data depicted in Fig. 1: Al–0.6 at. % Mg–1 at. % Zn (●) and Al–1.2 at. % Mg–2.5 at. % Zn (○).

These data can be compared with theoretical predictions obtained from Mott–Nabarro's model of solid solution hardening.[5–7] The effective obstacle spacing is given by

$$l_s = (4\mu b/\tau_i l)^{2/3} l, \tag{4}$$

where the maximum internal stress averaged over the space of radius $l/2$ around each solute is

$$\tau_i = \mu|\delta| c \ln 1/c. \tag{5}$$

Here $|\delta|$ represents the misfit parameters 0.02(Zn) and 0.1(Mg), respectively, and in the localized-force model l is related to the atomic fraction concentration c of solute by $l = b/\sqrt{2c}$. From Eq. (4) the averaged l_s is calculated for the two ternary alloys, assuming that the contributions of Mg and Zn are weighted by the corresponding fractions of their effective planar densities. The calculated values are listed in Table II and are in good agreement with the NMR experiments. It turns out that Friedel's model, in which a dislocation released at one impurity must, on the average, pick up exactly

TABLE II. Experimental observation and theoretical prediction of the effective solute spacing l_s (μm).

Sample	(Experiment) NMR	(Theory) Mott–Nabarro
Al–0.6 at. % Mg–1 at. % Zn	0.10	0.11
Al–1 at. % Mg–2.5 at. % Zn	0.07	0.05

one other one, is in conflict with the present investigation. The same conclusion has been drawn in the case of dilute Al–Mg and Al–Zn binary alloys.[8,9]

According to our assumption λ_F is the effective separation of forest dislocations in the solid without solute atoms and has the same strain dependence in the alloy as in the ultrapure material. Further, l_s is assumed to be independent of strain. Consequently, assuming the same evolution of the dislocation structure with increasing strain in ultrapure Al as in alloyed Al, then, according to Eq. (3) in the presentation of Fig. 4, the data of the alloyed Al should lead to straight lines parallel to the identity curve of Al (5*N*). As the deformed Al–0.6 at. % Mg–1.0 at. % Zn shows a dislocation cell structure that looks similar to the cell structure of deformed ultrapure Al [Fig. 2(a)], one expects such a behavior for Al–0.6 at. % Mg–1 at. % Zn. This is indeed confirmed by the experimental findings depicted in Fig. 4. It is in sharp contrast to the data of Al–1.2 at. % Mg–2.5 at. % Zn, which is not unexpected, as a matter of course, since no cell structure formation has been observed in the latter alloy. So, one should not expect to find $L_{\mathrm{NMR}}{}^{-1}$ of this alloy system to be parallel to $L_{\mathrm{NMR}}{}^{-1}$ of the ultrapure Al. Although its deviation is in line with the TEM observation in a qualitative sense, one might ask whether there exists a quantitative agreement regarding the strain dependence of $L_{\mathrm{NMR}}{}^{-1}$ of these alloy systems.

The physical picture that emerges is the following: when primaries move through a random field of solute atoms before encountering forest dislocations, the dislocation mobility is decreased relative to that possible at the same stress level compared to ultrapure material. In order to keep up with a fixed applied strain rate $\dot{\epsilon}$, the dilute alloy will have ρ_m greater than for the pure crystal. Consequently, at a corresponding strain the alloy has to have a higher stress level than the ultrapure crystal. This means that the effective obstacle spacing λ_F in the alloy will become smaller than λ_F observed in the ultrapure material since the effective flow stress is related to λ_F by

$$\sigma = \alpha\mu b\sqrt{\rho_F} \quad \text{and} \quad \lambda_F \sim 1/\sqrt{\rho_F}\,. \tag{6}$$

Now, the rate at which the decrease of L_{NMR} with increasing strain happens, depends considerably on the strain hardening Θ. According to Eq. (6),

$$\Theta = \frac{\delta\sigma}{\delta\epsilon} = \frac{\alpha\mu b}{2\sqrt{\rho}}\left(\frac{\delta\rho}{\delta\epsilon}\right). \tag{7}$$

Although there exists some discussion about Eq. (7) as to whether the effective flow stress is controlled by intersection between primaries or forest dislocation densities, experimental work suggests that σ is controlled by forest dislocations or that forest contributions are always in a constant ratio independent of the dislocation

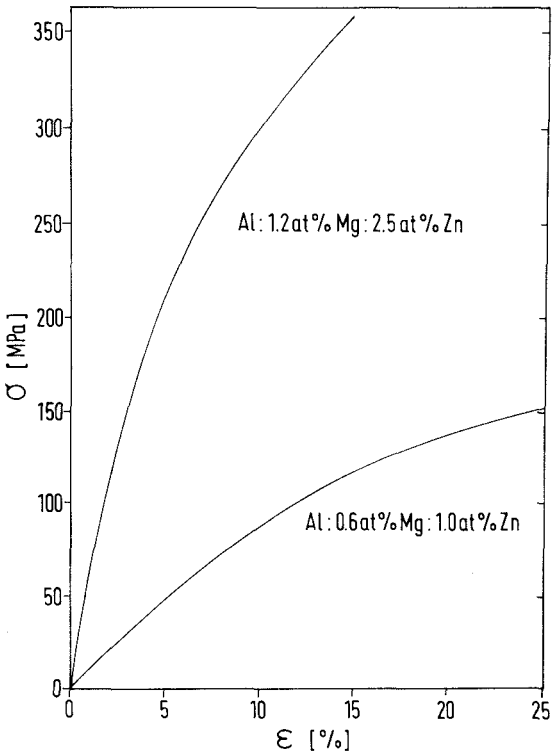

FIG. 5. Stress–strain curve at 77 K of Al–0.6 at. % Mg–1 at. % Zn and Al–1.2 at. % Mg–2.5 at. % Zn.

distribution.[10] The rate of change of dislocation density with strain in Eq. (7) is equal to $1/bL$, assuming that the mean free path is proportional to the mean jump distance L; i.e., Eq. (7),

$$1/L \sim \sqrt{\rho}\,\Theta\,. \tag{8}$$

At the beginning of deformation (stage-2 in polycrystalline materials) $\sqrt{\rho}$ is proportional to $\Theta\epsilon$. As a result, the inverse of the jump distance $1/L$ is proportional to $\Theta^2\epsilon$. Taking the work-hardening rates of the two alloys from Fig. 5, the ratio $\Theta_{\mathrm{II}}/\Theta_{\mathrm{I}}$ is found to be 2.2 at 6% strain. Therefore one should expect that

$$L_{\mathrm{I}}/L_{\mathrm{II}} = (\Theta_{\mathrm{II}}/\Theta_{\mathrm{I}})^2 = 4.8\,, \tag{9}$$

where I refers to Al–0.6 at. % Mg–1 at. % Zn and II refers to Al–1.2 at. % Mg–2.5 at. % Zn. Indeed, this is confirmed by Fig. 4, where $1/L_{\mathrm{II}}$ is found to be about five times larger than $1/L_{\mathrm{I}}$ at $\epsilon = 6\%$. So, there is an internal consistency between the mean jump distance measured by NMR and the macroscopic stress–strain dependence. In addition, there exists an internal consistency between the mean jump distance measured by NMR as a function of strain and the transmission electron microscopic observations of these alloys [Figs. 2(b), 2(c)]. In alloy I (Al–0.6 at. % Mg–1 at. % Zn) a cell structure developed. This means that the dislocation cells shrink in size through the subdivision of the

larger cells in the beginning. Since subdivisions cease, the cells have become so small that no new cell walls are being nucleated because chance encounters of glide dislocations have become negligibly small. Therefore the shrinking process of the cell pattern cannot go indefinitely and the cell diameter approaches an asymptotic value. After the cells have been established, the work-hardening rate will be small since the slip distance of the dislocations will be constant when crossing equally sized cells. When there is no cell structure developed like in alloy–II (Al–1.2 at. % Mg–2.5 at. % Zn), the work-hardening rate is not constant but increasing compared to pure Al, leading to a sharper decrease of the mean jump distance in this alloy as a function of strain. As a consequence, $1/L_{\mathrm{I}}$ vs ϵ should be parallel to the $1/L$ (pure Al) vs ϵ, but $1/L_{\mathrm{II}}$ vs ϵ should increase steeply compared to pure Al.

IV. CONCLUSION

Nuclear spin relaxation measurements in the rotating frame are shown to be a powerful tool for studying dislocation dynamics in ternary Al–Mg–Zn alloys. In particular, the experiments provide detailed information of the mean jump distance of mobile dislocations in these alloys. It turned out that in highly deformed samples the obstacles to moving dislocations are forest dislocations whereas in undeformed samples the barriers are forest dislocations and solute atoms as well. The mean jump distances measured by NMR at small strain values are in agreement with predictions based on Mott–Nabarro's model of solid solution hardening. At large strain, the jump distances measured by NMR are consistent with the TEM observations of the dislocation spacings and with the macroscopic stress–strain dependence of these alloy systems.

ACKNOWLEDGMENTS

This work is part of the research program of the Foundation for Fundamental Research on Matter (FOM–Utrecht) and has been made possible by financial support from the Netherlands Organization for the Advancement of Pure Research (ZWO–The Hague) and the Deutsche Forschungsgemeinschaft, Federal Republic of Germany.

REFERENCES

[1]E. Orowan, Z. Phys. **89**, 634 (1934).
[2]J. Th. M. De Hosson, O. Kanert, and A. W. Sleeswyk, in *Dislocations in Solids*, edited by F. R. N. Nabarro (North-Holland, Amsterdam, 1983), Vol. 6, Chap. 32, pp. 441–534.
[3]H. Tamler, O. Kanert, W. H. M. Alsem, and J. Th. M. De Hosson, Acta Metall. **30**, 1523 (1982).
[4]H. J. Hackelöer, O. Kanert, H. Tamler, and J. Th. M. De Hosson, Rev. Sci. Instrum. **54**, 341 (1983).
[5]F. R. N. Nabarro, *The Physics of Metals II, Defects*, edited by P. B. Hirsch (Cambridge U.P., Cambridge, 1975), p. 152.
[6]F. R. N. Nabarro, Philos. Mag. **35**, 613 (1977).
[7]F. R. N. Nabarro, *Dislocations and Properties of Real Materials* (Institute of Metals, London, 1985), p. 152.
[8]J. Th. M. De Hosson, G. Boom, U. Schlagowski, and O. Kanert, Acta Metall. **34**, 1571 (1986).
[9]U. Schlagowski, O. Kanert, J. Th. M. De Hosson, and G. Boom, Acta Metall. **36**, 865 (1988).
[10]P. B. Hirsch, *Physics of Metals II*, edited by P. B. Hirsch (Cambridge U.P., Cambridge, 1975), p. 189.